Available online at www.sciencedirect.com
SCIENCE DIRECT®
Journal of Solid State Chemistry 177 (2004) 1416–1424
JOURNAL OF SOLID STATE CHEMISTRY
http://elsevier.com/locate/jssc

Electrosynthesis and crystal structure of the new 15R hexagonal perovskite $Ba_5MnNa_2V_2O_{13}$

Abdelaziz Bendraoua,[a,b] Eric Quarez,[b] Francis Abraham,[b] and Olivier Mentré[b,*]

[a] *Laboratoire de Physico-chimie des Matériaux, USTOran, Algeria*
[b] *Laboratoire de Cristallochimie et, Physicochimie du Solide, UMR CNRS 8012, ENSCL, Université des Sciences et Technologies de Lille, B.P. 108, 59652 Villeneuve d'Ascq Cedex, France*

Received 15 September 2003; received in revised form 12 November 2003; accepted 23 November 2003

Abstract

A new manganese oxide $Ba_5MnNa_2V_2O_{13}$ with an original structure closely related to the cubic perovskite has been prepared by electrosynthesis in molten NaOH. Its crystal structure has been refined from single crystal X-ray diffraction in the $R\bar{3}m$ space group, $a = 5.8490(6)$ Å, $c = 36.856(5)$ Å, $Z = 3$, $R_1 = 4.72\%$, w$R_2 = 10.56\%$. The crystal structure is a rhombohedral 15R polytype and exhibits a close packed structure built up from $[BaO_{3-\delta}]$ (c) and $[BaO_2]$ (c') layers within a $(ccc'cc)_3$ stacking sequence. The resulting three-dimensional edifice is formed by $Ba(Mn_{0.33}Na_{0.67})O_3$ cubic perovskite blocks separated by double sheets of $V^{5+}O_4$ tetrahedra pointing towards the central $[BaO_2]c'$ layer. In the perovskite blocks, 1/6 of oxygen deficient vacancies located on layers surrounding manganese involve a Mn(IV) valence, in square pyramids rather than octahedra. On the same layers along c, the barium atom split from a central $(0, 0, z)$ position to close $(x, -x, z)$ positions as a compensation of the oxygen deficiency. In this work, a review of the Mn-related perovskite materials found in the literature is reported showing the wide variety of materials adopting related structural polytypes. A building scheme from simple to more complex edifices is also presented by successive intercalation of $[BaO_n]$ ($n = 1, 2$) in order to visualize topological relationships between the number of possible hexagonal perovskite series members.

Keywords: Electrosynthesis; Hexagonal perovskite; Layers stacking; Manganese oxides

1. Introduction

Electrocrystallization in molten alkali-hydroxide has recently shown a renewed interest since it possibly leads to the preparation of materials with high valence metals in solids, e.g., crystal growth of large $KBi^{V}O_3$ single crystals [1,2]. The recent use of this technique in our group also highlighted the possibility to prepare new materials in a more or less reproducible way as evidenced by the synthesis and characterization of the high Cu^{3+}/Ni^{3+} containing $Ba_2Na(Ni,Cu)_3^{2.33+}O_6$ [3] previously prepared using barium or sodium peroxide for the oxidizing agent [4,5]. The electrosynthesis of Ba–Ru-based chemical systems led to new hexagonal perovskites such as the 6H-$Ba_3Ru_2^{5.5+}NaO_9$ [6,7], 10H-$Ba_5Ru_3^{5.33+}Na_2O_{14}$ [8] and 12H-$Ba_6Ru_2^{5+}Na_2X_2O_{17}$ (X=V, Cr, Mn, P, As) [9]. The description of hexagonal perovskites crystal structure based on a close packing of AO_3 and deficient $AO_{3-\delta}$ layers allows one to generate an unlimited number of polytypes characterized by the n number of layers stacked along c; $n-$L (layers), $n-$H (hexagonal symmetry) or $n-$R (rhombohedral symmetry). The polytype structure is related to the ratio of cubic (c) and hexagonal (h) layers which itself depends on several factors such as the oxygen content and the cationic size. The most astonishing example is the large number of $BaMnO_{3-\delta}$ varieties stabilized for different δ values. Thus it has been shown that the 2H-$BaMnO_3$ is modified during the reduction process by means of the introduction of $BaO_{2.50}$ cubic layers yielding the 15R-$BaMnO_{2.90}$, 8H-$BaMnO_{2.875}$, 6H-$BaMnO_{2.833}$, 10H-$BaMnO_{2.80}$, 4H-$BaMnO_{2.75}$ [10–12], 21R-$BaMnO_{2.92-2.88}$ [13]. Furthermore the cationic substitution for Mn adds an additional degree of modification, e.g., the oxygen deficient 6H′ $BaMn_{1-x}Fe_xO_{3-\delta}$ [14] and the 9R "Bi–Sr"-stabilized $BaMnO_3$ [15]. Taking account of the special manganese

*Corresponding author. Fax: +33-0320436814.
E-mail address: mentre@ensc-lille.fr (O. Mentré).

0022-4596/$ - see front matter © 2003 Elsevier Inc. All rights reserved.
doi:10.1016/j.jssc.2003.11.022

adaptability, it was tempting to proceed electrosyntheses in Ba–Mn containing systems. It successfully led to several new materials including the title compound which is structurally characterized in this work. Taking into account the large number of manganese containing hexagonal perovskite, a special effort has been provided to list most of them, so-enabling to grasp the wide extent of this family of materials. Topological relationships was also established starting from the simple 2H and 3C to understand the building of more complex edifices including the 15R-$Ba_5MnNa_2V_2O_{13}$.

2. Experimental

2.1. Synthesis

Single crystals of $Ba_5MnNa_2V_2O_{13}$ were grown by electrosynthesis as previously described for several materials prepared in our laboratory [3,6,8,9]. NaOH was used as an oxidizing electrolyte particularly well-suited because of its low melting point (320°C). NaOH (pellets), $Ba(OH)_2 \cdot 3H_2O$, MnO_2, V_2O_5 in 10/0.5/0.5/0.5 proportions (g) were mixed and molten in an alumina crucible batch, set in quartz cell heated at 600°C in a vertical tubular furnace under flowing air. The temperature is controlled at the melt level using a standard *K*-type thermocouple. In the liquid, a constant potential (= 2.2 V) has been applied between a nickel and a zirconium foils playing the anode and cathode role, respectively. After a 24 h reaction, single crystals were extracted and water-washed from the deposited material at the cathode. Only few single crystals corresponding to the tittle compound could be isolated from the melt mixture. One must also notice that electrosynthesis using same experimental conditions permitting $Ba_5MnNa_2V_2O_{13}$ preparation has been hardly reproduced. Moreover, None of the number of attempts performed to prepare the title compound and isomorphous materials by solid-state reaction under different experimental conditions such as heating in air, flowing N_2, or NaOH flux lead to the expected material as summarized in Table 1. The reactants are $BaCO_3$, $Ba(OH)_2 \cdot 3H_2O$, V_2O_5, MnO_2, Mn_2O_3, TiO_2. It is also worth remarking that the $Ba_5MnNa_2V_2O_{13}$ phase is not stable in air since the single crystals deteriorate after two months exposure.

2.2. Single crystal X-ray diffraction study

Single crystal X-ray diffraction data were collected using a SMART-1K CCD detector BRUKER diffractometer under the conditions given in Table 2. A total of 3×600 frames have been collected (ω-scans, 10 s. per frame, 0.3° oscillations for three different values of φ: 0°, 120° and 240°) with a crystal-detector distance of 45 mm. The intensity data have been extracted from the collected frames using the program Saint Plus 6.02 [16]. An absorption correction based on the faces indexation have then been applied using the program Xprep of the SHELXTL package [17]. Data were then corrected for the glass fiber and the area detector absorption using non-theta dependent empirical corrections ($\mu \times r = 0$) with the program SADABS [18]. 2394 measured reflections have been merged in 339 independent reflections in the $\bar{3}m$ Laue group leading a $R_{int} = 4.52\%$.

3. Results and discussion

3.1. X-ray diffraction refinement

The crystal structure of $Ba_5MnNa_2V_2O_{13}$ was satisfactorily refined in the hexagonal orientation of the $R\bar{3}m$ space group using the SHELXTL package [17]. The Patterson function calculation yields the location of barium atoms in three sites (both Ba(1) and Ba(2) in (6*c*): 0, 0, $z \sim 0.30$; 0, 0, $z \sim 0.09$ and Ba(3) in (3*b*): 0, 0, 0.5). Coordinates and isotropic displacement parameters are refined yielding $R_1 = 31.91\%$ ($wR_2 = 68.81\%$). Fourier difference syntheses reveal three maxima: one in (3*a*) and two in (6*c*). According to their respective density, they are attributed to Mn, V and Na atoms. The consideration of these atoms, refinement converged to

Table 1
summary of the several attempts to prepare $Ba_5MnNa_2V_2O_{13}$ and isotypic materials

Expected compound	Thermal treatment(s)	Final compounds
$Ba_5MnNa_2V_2O_{13}$	N_2, 900–1100°C, →	Major $Ba_3(Mn/VO_4)_2$
$Ba_5MnNa_2V_2O_{13}$	Air, 500°C, →	$BaCO_3 + Ba_5(MnO_4)_3OH$
$Ba_5MnNa_2V_2O_{13}$	Air, 800°C, 1000°C, 1200°C, →	Major $Ba_3(Mn/VO_4)_2$
$Ba_5MnNa_2V_2O_{13}$	NaOH flux, 300–500°C, →	$Ba_3(Mn,V)_2O_8$ single crystals
$Ba_5MnNa_2P_2O_{13}$	Air, 800°C, →	Major $NaBa(P/MnO_4)$
$Ba_5TiNa_2V_2O_{13}$	Air, 800°, 1000°C →	Major $Ba_3(VO_4)_2$
$Ba_5TiNa_2P_2O_{13}$	Air, 800°C →	apatite $Ba_5(PO_4)_3O_{0.5} + NaBaPO_4$
$Ba_5RuNa_2V_2O_{13}$	Air, 800°C→	Major $Ba_6Ru_2V_2Na_2O_{17}$ (Ref. [9])
$Ba_5RuNa_2P_2O_{13}$	Air, 800°C→	Major $Ba_6Ru_2Na_2P_2O_{17}$ (Ref. [9])

Table 2
Crystal data, data collection and structure refinement parameters for $Ba_5MnNa_2V_2O_{13}$

Crystal data	
Color of Crystal	Dark brown
Symmetry	Trigonal
Space group	$R\bar{3}m$ (n°166)
Unit cell (Å)	a = 5.8490(6)
	c = 36.856(5)
Volume (Å^3)	1091.95(20)
Z	3
Calculated density (g/cm^3)	5.007
Data collection	
Equipment	Bruker SMART CCD-1K
Radiation MoKα (Å)	0.71073
Scan mode	ω - scan
Recording angular range 2θ (°)	3.32 – 65.68
Recording reciprocal space	$-8 \le h \le 4$
	$-6 \le k \le 8$
	$-52 \le l \le 52$
Number of measured reflections (I>½σ(I))	2394
Number of independent reflections (I>½σ(I))	388
Number of independent reflections (I>2σ(I))	339
μ (mm^{-1})	15.47
Limiting faces and distances (mm) from an arbitrary origin	0 0 1 0.005 0 0 $\bar{1}$ 0.028 0 2 $\bar{3}$ 0.060 0 $\bar{1}$ 1 0.057 $\bar{5}$ 4 2 0.014 3 $\bar{2}$ $\bar{1}$ 0.005
Transmission factor range	0.394 / 0.702
R merging factor	4.52
Refinement parameters	
Number of refined parameters / constraints	36 / 0
R_1 (F) [I>2σ(I)] $= \sum \lvert \lvert F_O \rvert - \lvert F_C \rvert \rvert / \sum \lvert F_O \rvert$ (%)	4.72
wR_2 (F^2) [I>2σ(I)] $= \left[\sum w(F_O^2 - F_C^2)^2 / \sum w(F_O^2) \right]^{1/2}$ (%)	10.93
$w = 1 / [\sigma^2(Fo^2) + (A \times P)^2 + B \times P]$ with $P = [\max(F_o^2 .0) + 2 F_c^2)] / 3$	A = 0.51 B = 9.25
Isotropic secondary extinction	Not refined
Max/Min Δρ.e Å^{-3}	1.75 / -1.65

$R_1 = 18.76\%$, $wR_2 = 49.52\%$. The subsequent Fourier difference synthesis permits to locate oxygen atoms in three sites: two in (18 h) positions ($x \sim 0.15$, $y = 2x$, $z \sim 0.03$ and $x \sim 0.16$, $y = 2x$, $z \sim 0.22$) and one in (6*c*) (0, 0, $z \sim 0.16$). The reliability factors converge to $R_1 = 12.86\%$, $wR_2 = 38.11\%$. The refined isotropic displacement parameters for all atoms did not reveal discrepancies, except for O(1) greater than expected ($U = 0.04$ Å^2). However, fully occupied oxygen sites involve unlikely Mn^{6+} in the compound. The refinement of the cationic occupancies yield fully occupied positions. The refinement of oxygen atoms sites revealed fully occupied sites for O(2) and O(3) while O(1) occupancy spontaneously converges to 0.83(2)(= 5/6) assorted with a minor decrease of reliability factors ($R_1 = 12.69\%$, $wR_2 = 37.84\%$). Anisotropic atomic displacement parameters for all atoms, and an optimized weighting scheme (see Table 2) have been introduced leading to $R_1 = 5.80\%$ ($wR_2 = 12.13\%$). At this stage, Ba(1) thermal parameter in the *xy* plane are abnormally high while a strong peak close to it is observed on Fourier difference maps. The splitting of this atom in

Table 3
Atomic parameters and thermal parameters U_{eq} for $Ba_5MnNa_2V_2O_{13}$ ($a = 5.8490(6)$, $c = 36.856(5)$, G. S. $R\bar{3}m$)

Atoms	Site	Occ.	x	y	z	U_{eq}[a] (Å^2)
Ba1	18*h*	1/3	0.0260(4)	0.0520(8)	0.30563(5)	0.0192(14)
Ba2	6*c*	1	0	0	0.09129(3)	0.0182(4)
Ba3	3*b*	1	0	0	$\frac{1}{2}$	0.0265(6)
Mn	3*a*	1	0	0	0	0.0147(11)
V	6*c*	1	0	0	0.20858(8)	0.0083(7)
Na	6*c*	1	0	0	0.5991(3)	0.019(2)
O1	18*h*	0.83(2)	0.153(1)	0.306(4)	0.027(3)	0.028(3)
O2	18*h*	1	0.1563(8)	0.3126(46)	0.2250(2)	0.022(2)
O3	6*c*	1	0	0	0.1628(4)	0.034(5)

[a] $U_{eq} = \frac{1}{3}\left(\sum_i \sum_j U_{ij} a_i * a_j * a_i a_j\right)$.

Table 4
Inter atomic distances (Å) and bond valences (ΣS_{ij}) for $Ba_5MnNa_2V_2O_{13}$

Ba1 Environment[*]		*Ba2 Environment*[*]	
Ba–O1 × 2	2.710(4)	Ba–O3 × 1	2.63(2)
Ba–O1 × 2	2.725(9)	Ba–O1 × 3	2.743(9)
Ba–O1 × 2	2.9282(6)	Ba–O2 × 6	2.991(2)
Ba–O1 × 1	2.980(10)	ΣS_{ij}	2.18
Ba–O1 × 2	3.167(4)	*Ba3 Environment*	
Ba–O2 × 1	3.241(9)	Ba–O2 × 6	2.808(8)
Ba–O2 × 2	3.436(9)	Ba–O3 × 6	3.380(5)
ΣS_{ij}	2.12	ΣS_{ij}	1.76
Na^+ Environment		*V^{5+} Environment*	
Na–O1 × (2–3)	2.29(1)	V–O3	1.69(2)
Na–O2 × 3	2.33(1)	V–O2 × 3	1.701(9)
ΣS_{ij}	1.25–1.51	ΣS_{ij}	5.32
Mn^{4+} Environmen			
Mn–O1 × 5	1.90(1)		
ΣS_{ij}	3.36		

[*]Valence bond sums for Ba1 and Ba2 are calculated taking account of fully occupied O1 positions.

three 18 h $(x, 2x, z)$ positions significantly improved the refinement convergence ($R1 = 4.72\%$). It is noticeable that Ba(1) stand at the same z coordinate that the deficient O(1) atom. The refined atomic coordinates and isotropic displacement parameters are presented in Table 3. The relevant bond lengths are listed in Table 4. Valence bond sums calculated using Brese and O'Keeffe's data [19] are also reported in Table 4.

3.2. Crystal structure description

$Ba_5MnNa_2V_2O_{13}$ crystal structure can be described by the stacking of three blocks of five $[BaO_3]$, $[BaO_{15/6}]$ and $[BaO_2]$ layers according to a $(ccc'cc)_3$ sequence where c' stands for *a*. $[BaO_2]$ layer. As shown in Fig. 1, the stacked cubic layers $[BaO(2)_3]$ and $[BaO(1)_{15/6}]$ with the ABCA sequence form perovskite blocks in which MnO_6 and NaO_6 octahedra share corners. In fact, the statistical occupancy of 5/6 for O(1) involves MnO_5 square planar pyramids and a mixture of NaO_6 (50%) and NaO_5 (50%) polyhedra. The resulting blocks are sandwiched by double sheets of VO_4 tetrahedra pointing towards the central c' $[BaO_2]$ layers as detailed in the discussion.

3.3. Distances and valence bond sums

Mn–O distances of 1.90(1) Å are typical of tetravalent manganese in an octahedral coordination, therefore the deficient O(1) position yields a ΣS_{ij} value of +3.36 instead of +4 which indicates minor relaxations over this site. The Ba(1) splitting around a central $(0, 0, z)$ position is in good agreement with the O(1) deficient nature, so-picturing a compact rearrangement of the layers. As shown by valence bond sums calculations, Ba1 and Ba2 are reasonably well-bonded considering Ba–O bonds up to 3.5 Å and fully occupied O1 positions. It is obvious that O1 deficiency yields relaxations in the concerned layers. Attempts to anticipate the 1/6 of vacancies location relatively to Ba1 is speculative, but considering the six surrounding Ba1–O bonds on the same layer (2×2.71 Å, 2×2.93 Å, 2×3.17 Å), a short Ba–O distance of 2.71 Å is likely insuring a more compact aspect of the layers, Fig. 2. The short Na–O bonds (2.29(1) Å–2.33(1) Å) are similar to

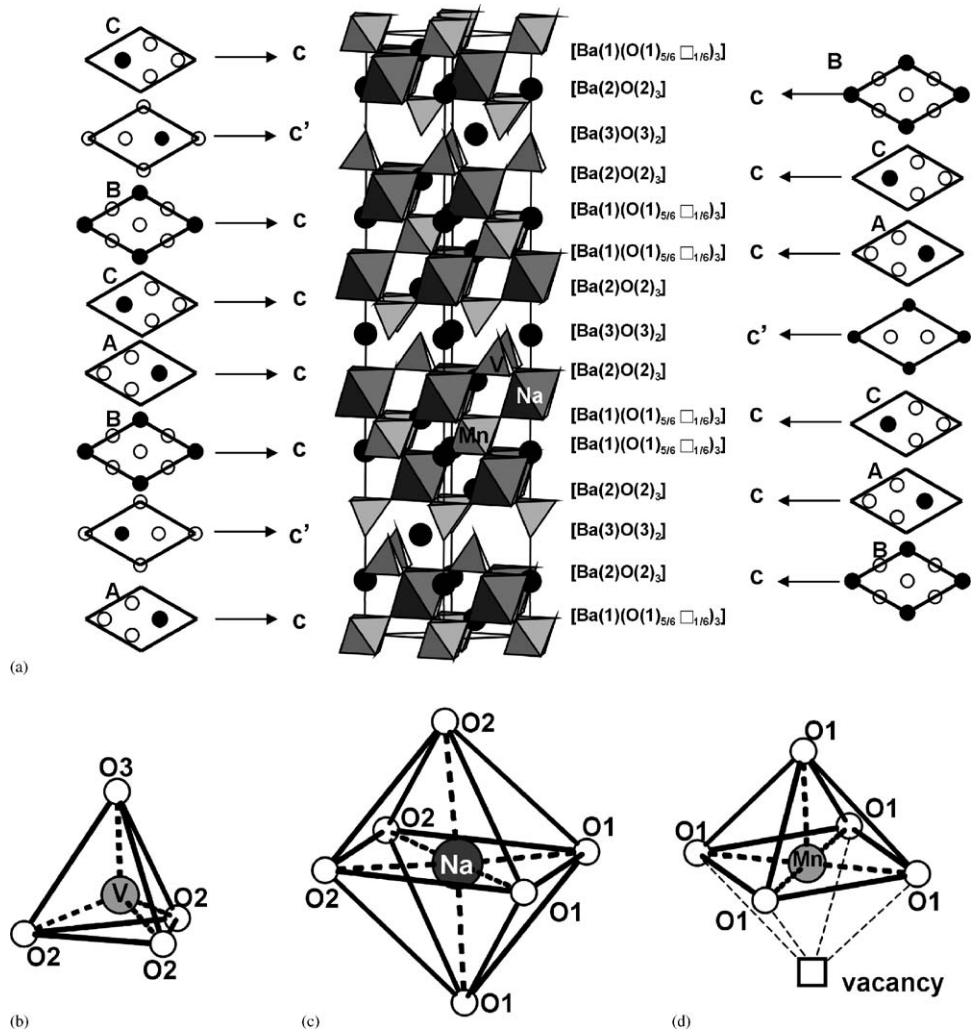

Fig. 1. Representation of the ideal $Ba_5MnNa_2V_2O_{13}$ crystal structure and $[BaO_3]$ and $[BaO_2]$ layers; Ba1 splitting and O1 vacancies are not drawn (a); environment of V (b), Na (c) and Mn (d). Note that half of the Na^+ are 5-coordinated because of O(1) lacunar positions.

those observed in ruthenium based hexagonal perovskites [6,8,9] which systematically lead to large values of valence bond sums. This feature is somewhat softened in our case by the presence of both 5- and 6-coordinated Na^+ yielding $\Sigma S_{ij} = 1.25$ and 1.51, respectively. The consequent constraints existing over the sodium positions may be due to its preference in perovskite-related materials to adopt a prismatic coordination as explained in Ref. [8]. The valence bond sum for vanadium in tetrahedral environment well confirms the 5+ oxidation state ($\Sigma S_{ij} = 5.27$).

3.4. Related compounds

The VO_4 tetrahedra arrangement in the tridimensional block is a direct consequence of the stacking sequence. As shown in Fig. 3(a), the replacement within a ABC stacked block of a cubic (c) $[AO_3]$ layer for a non-compact $[AO_2]$ layer induces the creation of pairs of tetrahedra pointing towards the oxygen deficient (c') layer. It is noteworthy that corner-sharing tetrahedra dimers, commonly observed in layer based oxides arise from the replacement within a AB stacking of a $[AO_3]$ hexagonal (h) layer for a deficient (h') [AO] layer, Fig. 3(b). Keeping in mind these rules, one can easily establish a topological relationship scheme leading to any possible material from: (i) a simple modification of the stacking sequence: previous studies have suggested that many factors, including the size (influence on the Goldsmith factor value), charge and coordination preference have a role to play in determining the adopted arrangement [20], (ii) the substitution of a compact layer for another one or a deficient non-compact one which is directly ruled by the material stoichiometry. So, starting from the cubic 3C perovskite (ABC sequence, (ccc) blocks), a number of compounds follows from the $[AO_3]$ substitution. Hexagonal [BaO]

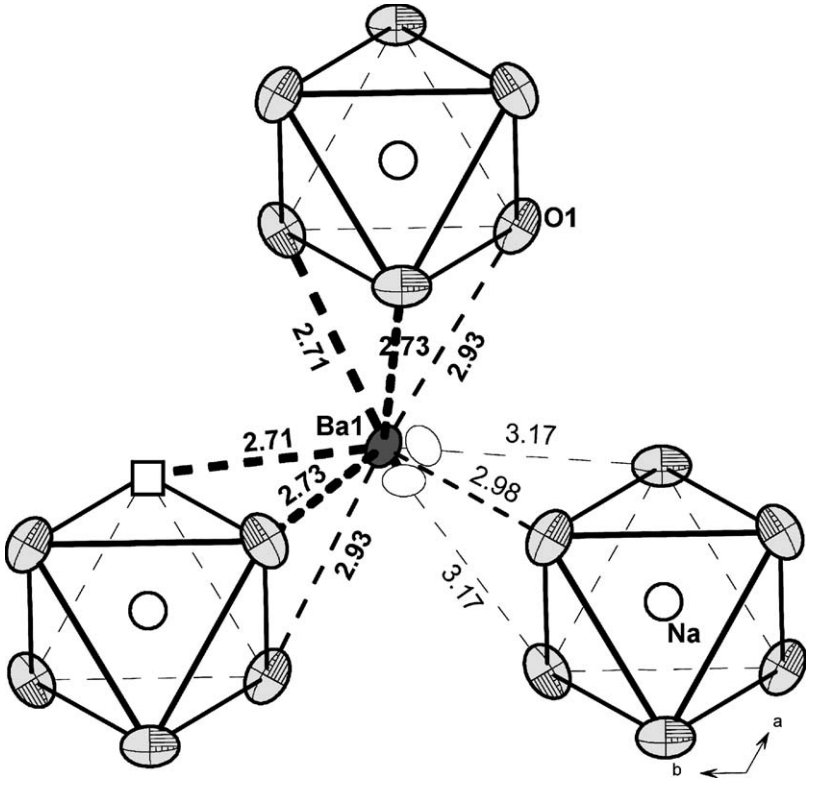

Fig. 2. The Ba_1 environment. On a layer along *c*, vacancies are suggested to exist close to Ba_1 for a homogeneous compactness.

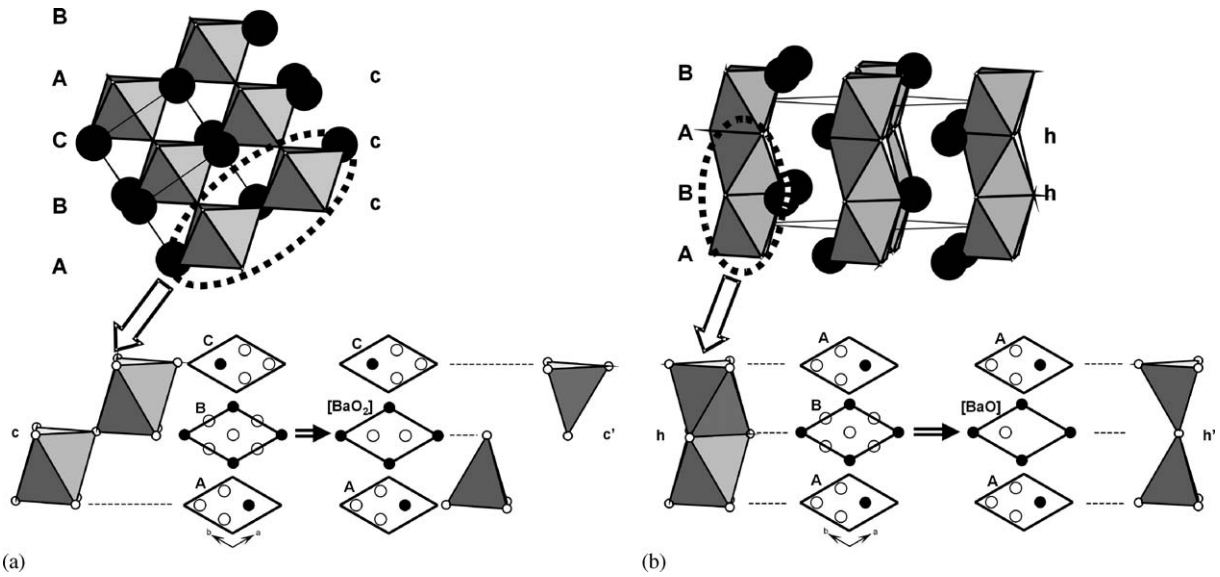

Fig. 3. Schematic representation of polyhedra obtained after replacing a BaO_3 layer by a BaO_2 layer in a stacking sequence typical of 3C cubic perovskite leading to isolated tetrahedra (a) and after considering same replacement by a BaO layer in a 2H hexagonal perovskite leading to corner sharing tetrahedra (b).

layers in the 10H–$Ba_5In_2Al_2ZrO_{13}$ form Al_2O_7 dimers double slices [21], Fig. 4a, while double slices of isolated VO_4 tetrahedra are located at both sides of the cubic BaO_2 layers in the title compound, Fig. 4b. Same modifications of the $BaMnO_3$ type 2H model (AB sequence, (*hh*) blocks) yield arrangements such as in $Ba_5Co_5ClO_{13}$ [22], Fig. 4c, and $Ba(Ir,Co)_1O_{2.83}$ [23,24], Fig. 4d. One should remark that in the former, the BaOCl layers behave as the BaO layers, so chloride ions are not considered in the tetrahedral apices. Obviously, various sequences based on the mixture of both (*h*) and (*c*) [AO_3] layers, e.g., 10H-$Ba_5W_3Li_2O_{15}$ [25,26] illustrated in Fig. 4e which is formed by cubic blocks isolated by hexagonal dimers, can also accept other

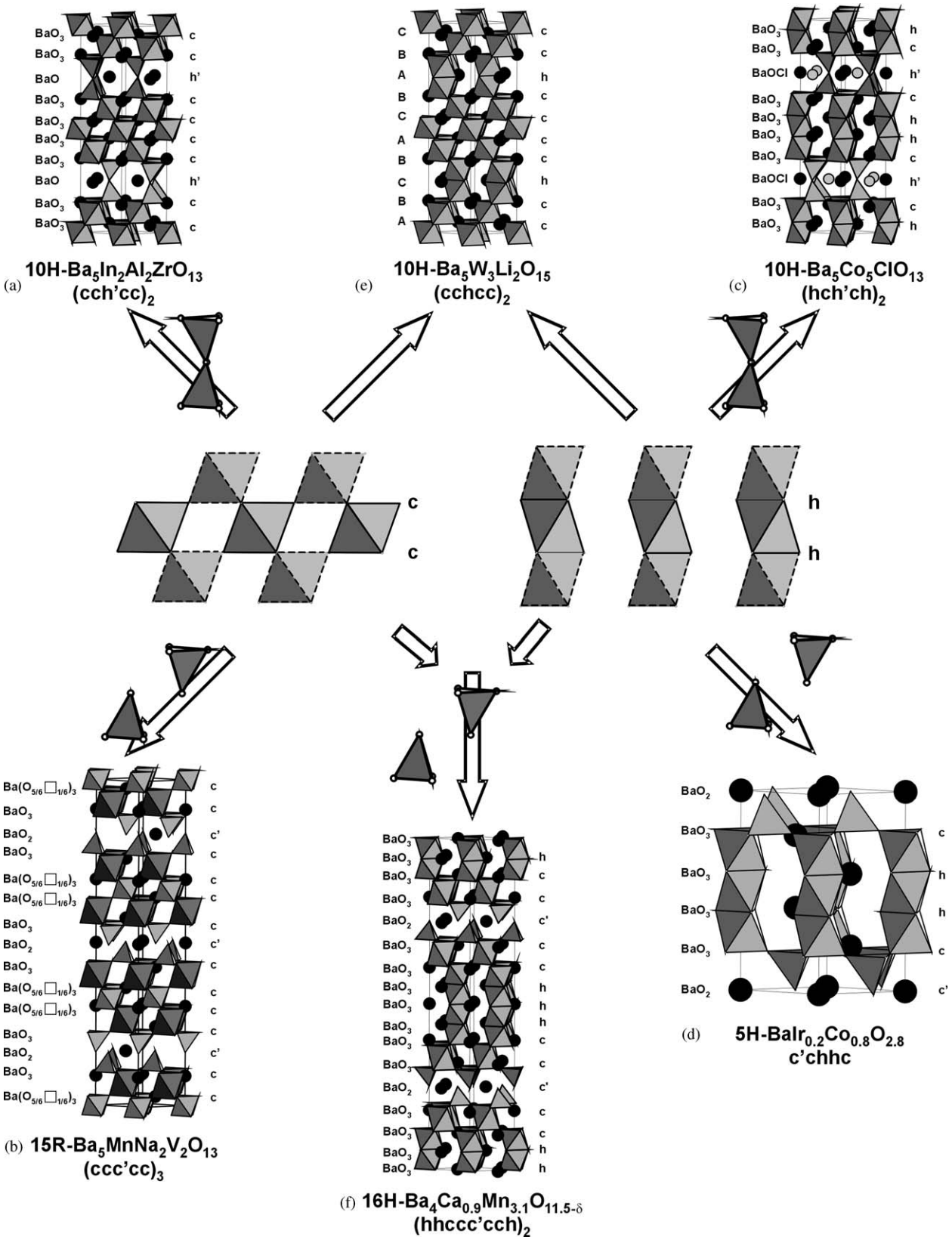

Fig. 4. Examples of structures built up from cubic and/or hexagonal blocks and double sheets of corner sharing/isolated tetrahedra.

Table 5
Reported Mn-perovskite related materials classified by stacking sequence

Structural type	Layers sequence	Compounds	Cell parameters (Å)	Space group	Ref.
Perovskites composed of $[AO_3]_c$ and/or $[AO_3]_h$ layers					
3C	*ccc*	$LaMn^{3+}O_3$	$a = 3.880$	$Pm\bar{3}m$	[28]
		$CaMn^{4+}O_3$	$a = 5.282$, $b = 5.266$, $c = 7.455$	$Pbnm$	[29]
2H	*hh*	$BaMn^{4+}O_3$	$a = 5.699$, $c = 4.815$	$P6_3/mmc$	[30]
4H	$(ch)_2$	$BaMn^{4+}O_3$ HT	$a = 5.669$, $c = 9.375$	$P6_3/mmc$	[31]
		$SrMn^{4+}O_3$	$a = 5.443$, $c = 9.070$	$P6_3/mmc$	[32]
6H	$(chc)_2$	$Ba_3ErMn_2^{4.5+}O_9$	$a = 5.823$, $b = 10.099$, $c = 14.409$	$Cmc2_1$	[33]
	hhhchc	$Ba(Mn_{0.767}Fe_{0.233})^{3.74+}O_{2.87}$	$a = 5.687$, $c = 14.167$	$P\bar{6}m2$	[14]
		$BaMn^{3.74+}O_{2.87}$	$a = 5.683$, $c = 14.096$	$P\bar{6}m2$	[10–12]
9R	$(chh)_3$	$Ba_3(MnRu_2)^{4+}O_9$	$a = 5.723$, $c = 21.409$	$R\bar{3}m$	[34]
		$Ba_9(Ru_{3.2}Mn_{5.8})^{4+}O_{27}$	$a = 5.704$, $c = 21.255$	$R\bar{3}m$	[35]
		$BaMn^{4+}O_3$	$a = 5.663$, $c = 20.955$	$R\bar{3}m$	[15]
		$Ba_9(Ir_{3.2}Mn_{5.8})^{4+}O_{27}$	$a = 5.709$, $c = 21.319$	$R\bar{3}m$	[35]
10H	$(hchch)_2$	$BaMn^{3.62+}O_{2.81}$	$a = 5.680$, $c = 23.373$	$P6_3/mmc$	[10–12]
15R	$(chhhh)_3$	$BaMn^{3.96+}O_{2.98}$	$a = 5.681$, $c = 35.377$	$R\bar{3}m$	[10–12]
	$(chchc)_3$	$Sr(Mn_{0.9}Fe_{0.1})^{4+}O_3$	$a = 5.449$, $c = 33.804$	$R\bar{3}m$	[14]
21R	$(chhhhhh)_3$	$BaMnO_{3-\delta}^{3/4+}$	$a \sim 5.5$, $c \sim 49$	$R\bar{3}m$	[13]
Hexagonal perovskites-related+$[BaO_2]_{c'}$ layers					
9R	$(c'hh)_3$	$Ba_3Mn_2^{5+}\square O_8$	$a = 5.711$, $c = 21.444$	$R\bar{3}m$	[36]
16H	$(hhhccc'cc)_2$	$Ba_4Ca_{0.9}Mn_{3.1}^{4.13+}O_{11.3}$	$a = 5.800$, $c = 38.958$	$P\bar{6}m2$	[27]
21R	$(hhccc'cc)_3$	$Ba_7Ca_2Mn_5^{4.4+}O_{20}$	$a = 5.821$, $c = 51.359$	$R\bar{3}m$	[37]
+$[BaCl]_{h'}$ layers					
6H	*hhh'h'hh*	$Ba_6(Ru_{2.5}Mn_{0.5})^{4.67+}O_{12}Cl_2$	$a = 5.799$, $c = 14.853$	$P\bar{3}m1$	[38]
+$[Ca_2O]$ layers					
9R		$La_2Ca_2Mn^{4+}O_7$	$a = 5.617$, $c = 17.352$	$R\bar{3}m$	[39]
+ $[Ca_2O_2]$ layers					
9R		$La_2Ca_2Mn^{4+}O_6(O_2)$	$a = 5.633$, $c = 17.488$	$R\bar{3}m$	[39]

types of layers, leading for instance to the coexistence of tetramers and BaO_2-modified cubic blocks in the 16H-$Ba_4Ca_{0.9}Mn_{3.1}O_{11.3}$ compound [27], Fig. 4f. A short review of manganese-based compounds formed of cubic and hexagonal $[AO_3]$ layers + various $[A_x(O/Cl)_y]$ layers is presented in Table 5. This list is not exhaustive but at least allows one to dispose of a large bibliographic record in the manganese hexagonal perovskite research field. For $La_2Ca_2MnO_7$ and the oxo $La_2Ca_2MnO_6(O_2)$, no h/c sequence can be written considering the $[Ca_2O]$ and $[Ca_2O_2]$ layers characteristics [39].

References

[1] T.N. Nguyen, D.M. Giaquinta, W.M. Davisand, H.-C. zur Loye, Chem. Mater. 5 (1993) 1273.
[2] T.N. Nguyen, Ph.D. Dissertation, Massachusetts Institute of Technology, 1994.
[3] E. Quarez, M. Huvé, P. Roussel, O. Mentré, J. Solid State Chem. 165 (2002) 214.
[4] M. Strunk, Hk. Müller-Buschbaum, Z. Anorg. Allg. Chem. 619 (1993) 343.
[5] G. Tams, Hk. Müller-Buschbaum, Z. Anorg. Allg. Chem. 617 (1992) 19.
[6] E. Quarez, M. Huvé, F. Abraham, O. Mentré, Solid State Sci. 5 (2003) 951.
[7] K.E. Sitzer, M.D. Smith, W.R. Gemmill, H.-C. Zu Loye, J. Am. Chem. Soc. 124 (2002) 13877.
[8] E. Quarez, O. Mentré, Solid State Sci. 5 (2003) 1105.
[9] E. Quarez, F. Abraham, O. Mentré, J. Solid State Chem. 176 (2003) 137.
[10] T. Negas, S. Roth, J. Solid State Chem. 3 (1971) 323.
[11] M. Parras, J. Alonso, J.M. Gonzàlez-Calbet, M. Vallet-Regi, Solid State Ionics 106 (1993) 614.
[12] J.M. Gonzàlez-Calbet, M. Parras, J. Alonso, M. Vallet-Regi, J. Solid State Chem. 106 (1993) 99.
[13] M. Parras, J.M. Gonzàlez-Calbet, J. Alonso, M. Vallet-Regi, J. Solid State Chem. 113 (1994) 78.
[14] V. Caignaert, M. Hervieu, B. Domengès, N. Guyen, J. Pannetier, B. Raveau, J. Solid State Chem. 73 (1988) 107.
[15] Ph. Boullay, M. Hervieu, Ph. Labbé, B. Raveau, Mater. Res. Bull. 32 (1997) 35.
[16] SAINT + ver. 6.02: Area-Detector Integration Software, Siemens Industrial Automation, Inc., Madison, WI, 1998.
[17] G.M. Sheldrick, SHELXTL NT ver. 5.1, Bruker Analytical X-ray Systems, 1998.
[18] SADABS, Area-Detector Absorption Correction, Siemens Industrial Automation, Inc., Madison, WI, 1996.
[19] M.E. Brese, M. O'Keeffe, Acta Crystallogr. B 47 (1991) 192.
[20] M.T. Anderson, K.B. Greenwood, G.A. Taylor, K.R. Poeppelmeier, Prog. Solid State Chem. 22 (1993) 197.
[21] R.V. Shpanchenko, A.M. Abakumov, E.V. Antipov, L.M. Kovba, J. Alloys Compounds 206 (1994) 185.
[22] K. Yamaura, D.P. Young, T. Siegrist, C. Besnard, C. Svensson, Y. Liu, R.J. Cava, J. Solid State Chem. 158 (2001) 175.
[23] J.F. Vente, P.D. Battle, J. Solid State Chem. 152 (2000) 361.

[24] H.U. Schaller, S. Kemmler-Sack, A. Ehmann, J. Less-Common Met. 97 (1984) 299.
[25] A.J. Jacobson, B.M. Collins, B.E.F. Fender, Acta Crystallogr. B 30 (1974) 816.
[26] E.F. Jendrek, A.D. Potoff, L. Katz, J. Solid State Chem. 14 (1975) 165.
[27] N. Floros, C. Michel, M. Hervieu, B. Raveau, Chem. Mater. 12 (2000) 3197.
[28] S. Naray-Szabo, Naturwissenschaften 31 (1943) 466.
[29] H. Taguchi, J. Solid State Chem. 124 (1996) 360.
[30] E.J. Cussen, P.D. Battle, Chem. Mater. 12 (2000) 831.
[31] A. Hardy, Acta Crystallogr. 15 (1962) 179.
[32] P.D. Battle, T.C. Gibb, C.W. Jones, J. Solid State Chem. 74 (1988) 60.
[33] C. Rabbow, Hk. Müller-Buschbaum, Z. Naturforsch. 49b (1994) 1277.
[34] Z. Serpil Gönen, J. Gopalakrishnan, B.W. Eichhorn, R.L. Greene, Inorg. Chem. 40 (2001) 4996.
[35] S. Frenzen, Hk. Müller-Buschbaum, Z. Naturforsch. B: Chem. Sci. 50 (1995) 585.
[36] M.T. Weller, S.J. Skinner, Acta Crystallogr. C 55 (1999) 154.
[37] N. Floros, C. Michel, M. Hervieu, B. Raveau, J. Solid State Chem. 168 (2002) 11.
[38] M. Neubacher, Hk. Müller-Buschbaum, Z. Anorg. Allg. Chem. 602 (1991) 143.
[39] E. Gaudin, G. Goglio, A. Besnard, J. Darriet, J. Solid State Chem. 175 (2003) 124.